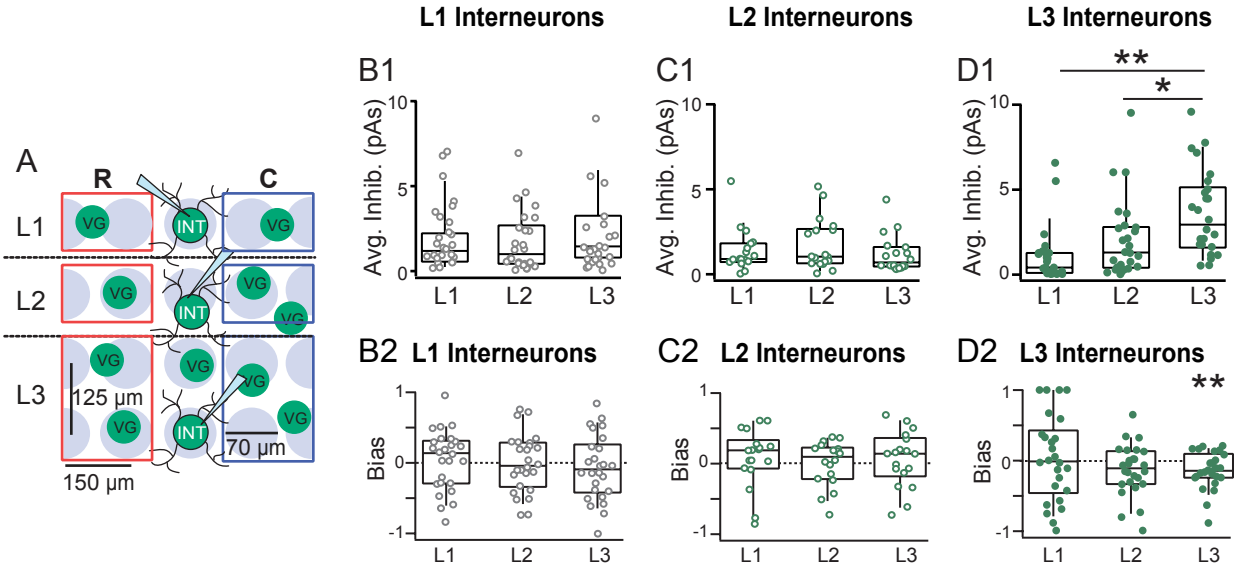

SI Figure 1: Laminar analysis of inhibitory strength and asymmetric bias in L1-3 Interneurons. A) Schematic of grid-stimulation paradigm for L1, L2 and L3 inhibitory interneurons. The inhibitory strength in each layer was taken average evoked IPSC area across all stimulation sites within the layer (5 sites in each L1, L2 and 10 sites in L3) as bounded by dashed lines. Inhibitory bias was calculated for each layer as the difference in average inhibition on caudal versus rostral sides divided by the sum of the average inhibition on either side as shown by the red and blue rectangles. B1) The average inhibition does not vary by layer in L1 interneurons. B2) In L1 interneurons, inhibition is not significantly asymmetric in any layer. C1) The average inhibition does not vary by layer in L2 interneurons. C2) In L2 interneurons, inhibition is not significantly asymmetric in any layer. (L1, L2, L3) are not asymmetric. D1) In L3 interneurons, the average inhibition is significantly greater from L3 than L2 (*<0.05) or L1 (**: $p<0.01$, ANOVA). D2) In L3 interneurons, inhibition is significantly asymmetric L3 (mean bias ≠ 0, one sample t-test, **$p<0.01$) and rostrally biased (bias<0).

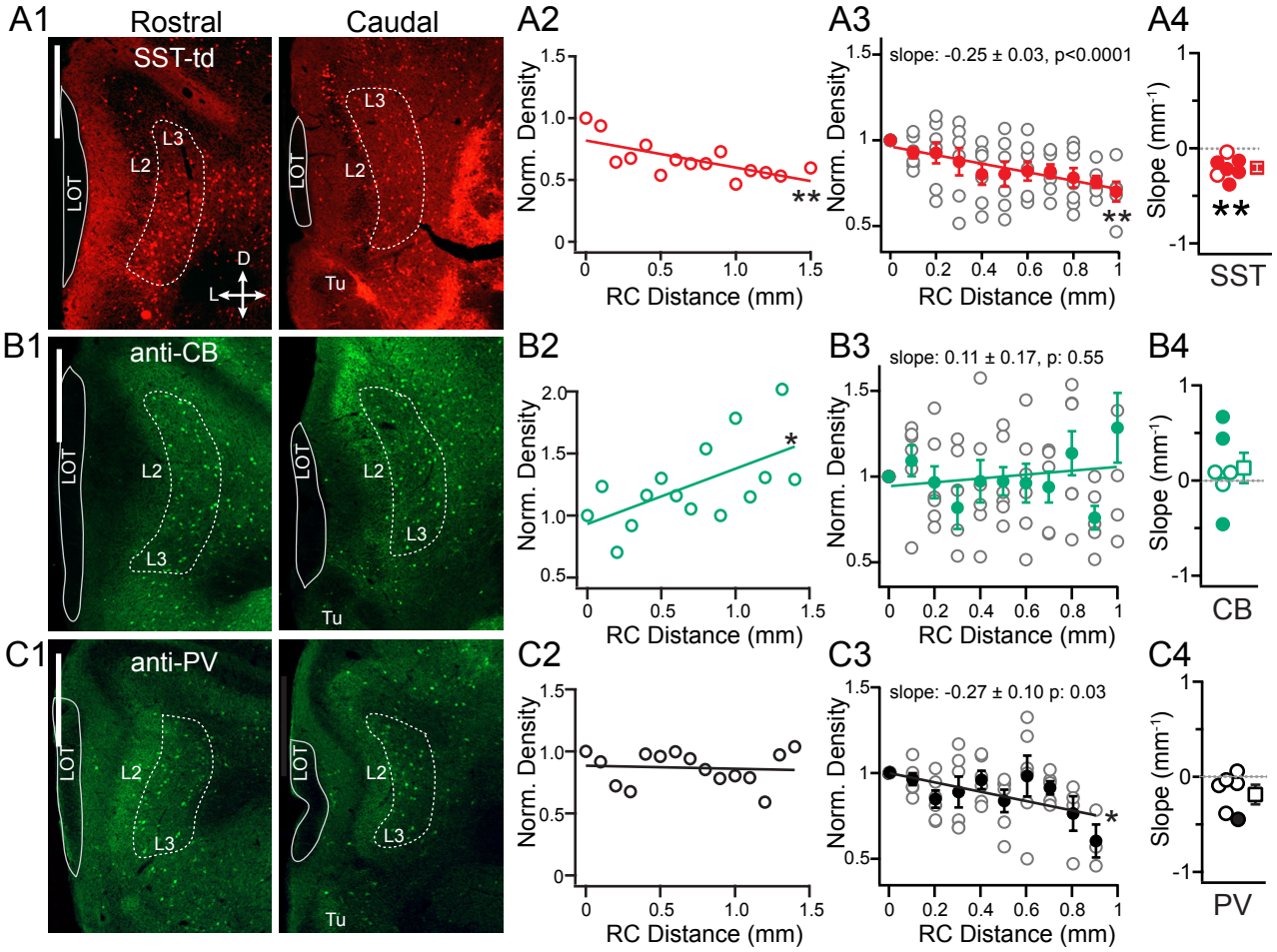

SI Figure 2: Rostral-caudal distributions of L3 interneurons. A1) Representative coronal sections from rostral (0-200 µm, left) and caudal (within last 300 µm, right) APC showing SST-tdTom(+) cells in L3 region of interest (ROI, dashed line). Scale bar: 500 µm A2) Normalized density versus RC distance for the mouse shown in A1 (SST-mouse #2, Table 1, ** p<0.01. A3) Normalized density of SST-cells versus distance for all mice (open circles). The average (± SE, n=7) normalized density of SST cells across mice significantly decreased with RC distance (red circles, **p<0.01). A4) Distribution of slopes from linear fits to data from individual mice. Solid circles indicate significantly negative slopes (p<0.05). The distribution of slope values was significantly non-zero (** p: 0.002 MWU-test). B1-4) As in A1-4, except for Calbindin(+) interneurons (CB). B1,2) Data from CB mouse #5 in Table 1. B3) On average, there is no change in density of CB cells along the RC axis (filled green circles, p: 0.55). B4) In individual mice CB cells significantly increased or decreased (filled green circles) along the RC axis, but the distribution of slopes did not differ from zero (p: 0.37, MWU-test). C1-4) As in A1-4, except for Parvalbumin(+) interneurons (PV). B1,2) Data from PV mouse #6 in Table 1. C3) On average, the density of PV cells decreased along the RC axis (filled black circles, p: 0.03). C4) However, only one mouse showed a significant decrease in PV cells along the RC axis (filled black circle) and the distribution of slopes did not differ from zero (p: 0.07, MWU-test).

	SST			PV			CB		
Mouse	Slope	R^2	P	Slope	R^2	P	Slope	R^2	P
1	**-0.13 ± 0.03**	**0.48**	**0.0014**	-0.07 ± 0.20	0.02	0.7385	0.08 ± 0.09	0.06	0.3827
2	**-0.22 ± 0.06**	**0.49**	**0.0038**	-0.09 ± 0.16	0.06	0.5977	0.09 ± 0.21	0.01	0.6787
3	-0.04 ± 0.03	0.10	0.2092	-0.38 ± 0.20	0.31	0.0950	**0.67 ± 0.21**	**0.47**	**0.0102**
4	**-0.24 ± 0.03**	**0.85**	**<0.0001**	0.06 ± 0.20	0.01	0.7621	**-0.47 ± 0.07**	**0.79**	**<0.0001**
5	**-0.15 ± 0.03**	**0.61**	**0.001**	**-0.44 ± 0.14**	**0.56**	**0.0124**	**0.44 ± 0.17**	**0.35**	**0.0212**
6	**-0.37 ± 0.05**	**0.86**	**<0.0001**	-0.02 ± 0.14	0.00	0.8698	-0.04 ± 0.10	0.01	0.6900
7	-0.27 ± 0.17	0.25	0.1402						
Fit Average	**-0.25 ± 0.03**	**0.88**	**<0.0001**	**-0.27 ± 0.10**	**0.46**	**0.0305**	0.11 ± 0.17	0.05	0.5538
Slope Dist ≠ 0	**-0.20 ± 0.04**	**-**	**0.0021**	**-0.16 ± 0.08**	**-**	**0.0658**	0.13 ± 0.16	-	0.3700

Supplemental Table 1: Linear regression slope values for fits to normalized density of three classes of interneuron versus RC distance in individual mice. Bold values correspond to significant ($p<0.05$) slope values (mm^{-1}). Linear regression was also performed on the average normalized density across mice versus distance for each interneuron class (Fit Average). P-values correspond to tests for slope not equal to zero. Finally, the distribution of slope values was compared to zero using a non-parametric Mann-Whitney test (distribution ≠ 0). SST- somatostatin interneurons, PV- parvalbumin interneurons, CB- Calbindin interneurons.

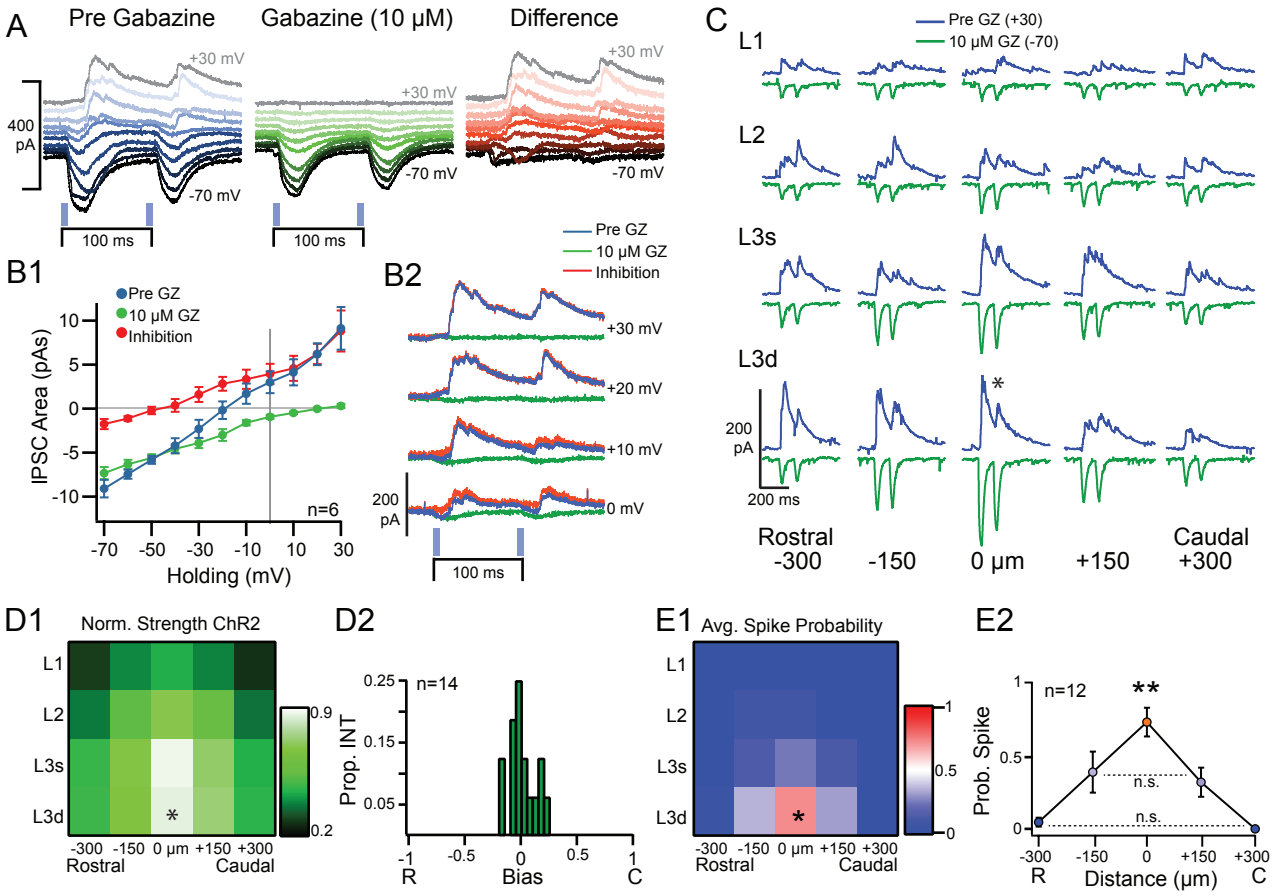

SI Figure 3: Influence of Channelrhodopsin activation on inhibition and spiking in L3 Interneurons. A) Mixed inhibitory and ChR2 currents (blue, left), isolated ChR2 currents (green, middle) and the difference corresponding to isolated inhibitory currents (red, right) recorded holding potentials from -70 mV (black) to +30 mV (gray) in 10 mV increments. B1) IPSC area under the first peak recorded as in (A). For total current (blue), ChR2 current (green) and the difference (isolated inhibition, red). Points represent Mean +/- SE over 6 interneurons. B2) Overlaid recordings from A for each condition at typical recording potentials for IPSCs. C) Response of neuron in A to grid stimulation pre (+30 mV) and post Gabazine (-70 mV) to reveal differential variation in inhibition and ChR2 activation over grid locations. Neuron is located at *. D1) Normalized ChR2 strength averaged across 14 neurons in response to grid stimulation. Neuron is located at *. D2) ChR2 currents do not show asymmetric responses. E1) Probability of spike response over grid location averaged over 12 neurons. E2) Spike probability is significantly higher for somatic stimulation (** $p<0.01$) and does not significantly differ for rostral versus caudal sites.

SI Methods: Spontaneous PSC detection algorithm

Custom analysis code was written in IgorPro (Wavemetrics) that combines a first-derivative threshold with template matching (Clements and Bekkers, 1997) to identify spontaneous PSCs. Examples of this analysis protocol are shown for recorded (SI Fig 4A, B) and simulated data (SI Fig 4C,D). First, mean subtracted, raw traces were smoothed (20 passes, fixed parameter) using a binomial filter and then duplicated (SI Fig 4A1, B1). One smoothed trace was differentiated to obtain the instantaneous slope (pA/s) at each point. A threshold was set at 4 standard deviations (SD) from the mean of the differentiated trace to identify events with the greatest instantaneous slopes that likely correspond to the largest PSCs (SI Fig 4A2, B2). The associated PSC events (60 ms duration) were extracted from the smoothed but undifferentiated trace and then averaged to obtain a template PSC that was normalized to 1 (SI Fig 4A3, B3 black traces). Then a second, lower threshold of 2SD was applied to the differentiated trace to identify all potential PSC events. For each event detected, the putative PSC event was extracted (60 ms duration). The amplitude of the event was taken as the peak current within 10 ms of event onset minus the average baseline 1 s prior to the event. The normalized template PSC was then scaled to this amplitude and subtracted from the putative PSC trace. The quality of the template match was quantified as the summed mean squared difference between the scaled template and the event. Matches with error values <0.3-0.5 (variable by dataset) were typically indicative of actual PSCs. Two additional exclusion criteria were included to ensure accurate PSC identification. First, identified PSCs must have width at half-max amplitude of >0.05 ms (fixed). Second, PSC amplitudes must be greater than the average deviation of the baseline preceding the event (~3-7 pA, variable by data set). All detected events that met criteria were considered PSCs (red or blue tags in SI Fig 4A1-D1), those that failed meet all three criteria were considered Non-events. We averaged all extracted traces each category to obtain the average PSC (Red or blue traces, SI Fig 4A3, B3) or Non-event waveform (gray traces). The non-event waveform in all data sets reflected the baseline noise, whereas the PSC waveform was highly similar to the template.

To evaluate the accuracy of PSC identification and measurement, we manually quantified the error rates of the analysis code on data sets from rostral and caudal cells (n=10 cells each, 20 s data per cell). Events identified as PSCs that were visibly inconsistent with the PSC template as false alarms (FA). Conversely, rejected events that were visibly consistent with the PSC template were counted as false rejections (FR). Finally, undetected events that were visibly consistent with the PSC template were counted as misses (M). These were then

summed to get the total error (TE) rate for each data set. The error rates did not significantly differ between rostral and caudal cells (SI Fig 4E). To evaluate analysis performance with respect to estimating PSC amplitude and frequency as well as error rates, we generated simulated data with known PSC amplitudes and frequency. Briefly, simulated data sets (200 s duration) were created by drawing event times from a Gaussian distribution with mean frequency of 9 Hz. Events were convolved with a real PSC template corresponding to PSCs recorded in representative rostral or caudal pyramidal cells. Simulated PSC amplitudes ranged from 5-25 pA consistent with the recorded cells and were drawn from a uniform distribution with mean amplitude of 14-16 pA. Finally, Gaussian noise was added to the entire trace (+/-10 pA). For simulated data (800 s total), PSC analysis returned mean PSC amplitudes with 96.2 ± 0.24% accuracy and PSC frequency with 95.7 ± 0.5% accuracy (SI Fig 4F1-3). The total error rate was 0.48 ± 0.02 Hz and parsed as follows: FA (0.076 ± 0.005 Hz), FR (0.13 ± 0.02 Hz) and M (0.25 ± 0.03 Hz). These error values are consistent with FA, FR, M and TE rates of real data (SI Fig 4E).

SI Figure 4: Evaluation of spontaneous PSC detection algorithm. **A1)** Representative traces from a rostral pyramidal cell (10 s total). Top: Example raw trace (red) the corresponding smoothed trace is immediately below (black). Subsequent smoothed traces from the same cell are shown below. Red markers correspond to identified sIPSCs. M: missed event, FA: false alarm, FR: false rejection. **A2)** Distribution of instantaneous slope values (pA/s) of the differentiated smoothed traces shown in A1. Black vertical line corresponds to 4SD from mean, red vertical line 2SD from mean. **A3)** Black: Template PSC averaged from events with slopes >4SD from the mean. Template PSC has been scaled to match the amplitude of the Mean PSC over all identified PSC events with slope >2SD from the mean (red). The mean Non-event is shown in gray. **B1)** As for A1, but for a representative caudal pyramidal cell. Blue markers correspond to identified sIPSCs. **B2)** Distribution of instantaneous slope values (pA/s) of the differentiated smoothed traces shown in B1. Black vertical line corresponds to 4SD from mean, blue vertical line 2SD from mean. **B3)** Black: Template PSC averaged from events with slopes >4SD from the mean. Template PSC has been scaled to match the amplitude of the Mean PSC over all identified PSC events with slope >2SD from the mean (blue). The mean Non-event is shown in gray. **C1-2)** As in A1 but for simulated data. **C3)** In this case the Template is that from the cell in A3 that was used to generate the PSCs in the simulated traces. **D1-2)** As in B1 but for simulated data. **D3**) In this case the Template is that from the cell in B3 that was used to generate the PSCs in the simulated traces. **E**) The average +/-SE rates for missed events (M), false rejections (FR), false alarms (FA) and total errors (TE) for rostral cells (n=10, 200 s total), caudal cells (n=10, 200 s total) and simulated data (n=4 simulations, 800 s total). The error rates between rostral and caudal cells did not significantly differ (paired t-test, p: 0.08-0.77). **F1-3)** Evaluation of the accuracy of the estimated (Est) mean PSC amplitude (F1) or frequency (F2) as a percentage (F3) of the actual mean values (Act) for simulated data. False alarm rates (E1) are subtracted from the estimated PSC frequency prior to obtaining the percent accuracy.

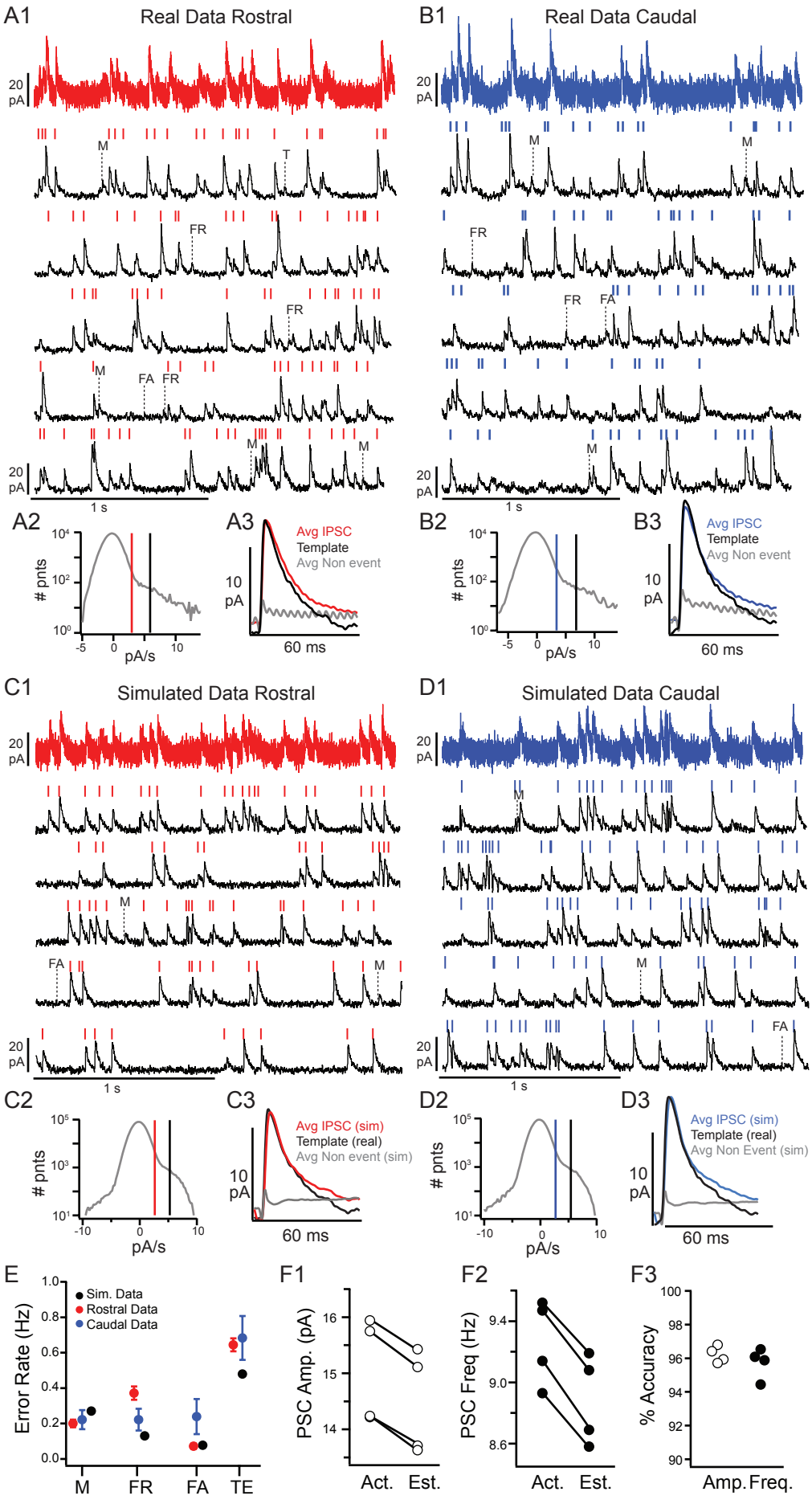
A1
Real Data Rostral
B1
Real Data Caudal
20 pA
M
T
FR
FA
1 s
A2
A3
B2
B3
pnts
pA/s
Avg IPSC
Template
Avg Non event
10 pA
60 ms
C1
Simulated Data Rostral
D1
Simulated Data Caudal
C2
C3
D2
D3
Avg IPSC (sim)
Template (real)
Avg Non event (sim)
Avg Non Event (sim)
E
Sim. Data
Rostral Data
Caudal Data
Error Rate (Hz)
M
FR
FA
TE
F1
F2
F3
PSC Amp. (pA)
PSC Freq (Hz)
% Accuracy
Act.
Est.
Amp.
Freq.